



LAWRENCE
LIVERMORE
NATIONAL
LABORATORY

Microstructural Evidence for Conditioning-dependent $(\delta) \rightarrow (\alpha)'$ Transformations in Retained (δ) -phase Pu-Ga

J. R. Jeffries, K. J. M. Blobaum, M. A. Wall, A. J.
Schwartz

June 17, 2008

Acta Materialia

Disclaimer

This document was prepared as an account of work sponsored by an agency of the United States government. Neither the United States government nor Lawrence Livermore National Security, LLC, nor any of their employees makes any warranty, expressed or implied, or assumes any legal liability or responsibility for the accuracy, completeness, or usefulness of any information, apparatus, product, or process disclosed, or represents that its use would not infringe privately owned rights. Reference herein to any specific commercial product, process, or service by trade name, trademark, manufacturer, or otherwise does not necessarily constitute or imply its endorsement, recommendation, or favoring by the United States government or Lawrence Livermore National Security, LLC. The views and opinions of authors expressed herein do not necessarily state or reflect those of the United States government or Lawrence Livermore National Security, LLC, and shall not be used for advertising or product endorsement purposes.

Microstructural Evidence for Conditioning-dependent $\delta \rightarrow \alpha'$ Transformations in Retained δ -phase Pu-Ga

J. R. Jeffries^{a,*} K. J. M. Blobaum^a M. A. Wall^a
A. J. Schwartz^a

^a*Lawrence Livermore National Laboratory, Livermore, CA 94550, USA*

Abstract

The retained δ phase of a Pu-1.9 at.% Ga alloy is metastable with respect to the martensitic $\delta \rightarrow \alpha'$ transformation that occurs at low temperatures. This transformation has been shown to proceed by means of an isothermal martensitic mode, but the kinetics of the transformation are atypical. The transformation exhibits a “double-C” in a time-temperature-transformation diagram, wherein there exist two temperatures where a given amount of transformation occurs in a minimum amount of time. The cause of the double-C kinetics remains uncertain, eliciting proposals of multiple mechanisms, multiple paths, or different morphologies as possible origins. Recently, a “conditioning” treatment was found to affect the $\delta \rightarrow \alpha'$ transformation, but the underlying mechanism by which the conditioning treatment influences the transformation has not yet been resolved. In this study, microstructural characterization as a function of temperature, time, and conditioning has been employed to illuminate the role of conditioning in the $\delta \rightarrow \alpha'$ transformation. Conditioning is found to enhance transformation in the upper-C and to enable transformation in the lower-C. The data garnered from these experiments suggest that conditioning is intimately linked to nucleation processes and of little consequence to the growth and morphology of the α' product phase.

Key words: Plutonium, phase transformation, martensite, metallography

PACS: 81.30.Bx, 81.30.Kf, 81.40.Ef

* Corresponding Author.

Email address: jeffries4@llnl.gov (J. R. Jeffries).

1 Introduction

Elemental plutonium is a material easily provoked from one stable or metastable state into another. Small perturbations in temperature, pressure, or doping have dramatic effects upon structural configurations and properties of this $5f$ -electron actinide element. Under ambient pressure and over a narrow temperature range from room temperature to its low melting point of 640 °C, unalloyed Pu exhibits six equilibrium crystal structures—the most of any pure element [1–4]. Within the multitude of structural phases, the low-temperature phases exhibit low-symmetry structures, rather than the high-symmetry, close-packed structures normally realized in elemental metals. The ductile δ phase, stable between 310 °C and 450 °C in unalloyed Pu, exhibits a high-symmetry, close-packed face-centered-cubic structure, yet this phase displays the lowest density of the six allotropes [5].

Further complicating our understanding of the phase diagrams of Pu and its alloys is the inherent radioactivity of Pu, the decay process most relevant to phase stability being the nuclear α -decay of the Pu atoms. This decay ejects a 5 MeV helium nucleus and an 86 keV uranium atom into the surrounding lattice, resulting in a significant damage cascade that generates thousands of Frenkel pairs within a 15 nm radius [6,7]. While many of these Frenkel pairs are thought to recombine at ambient temperatures, lattice damage can accumulate if a specimen is subjected to low temperatures [6,8]. In addition to defect damage, Pu self-irradiation induces the formation of helium bubbles as well as the generation of daughter products that alter the composition of the material. These radiation-induced effects conspire to prevent the attainment of true thermodynamic equilibrium in any radioactive Pu alloy [9].

Experimental data regarding the stability and properties of Pu at or near poorly understood phase transformations is of paramount importance to the development of accurate models encompassing f -electron physics and its ramifications. One such phase transformation, upon which little is tacitly agreed, is the low-temperature $\delta \rightarrow \alpha'$ transition in Pu-Ga alloys. Alloying Pu with small additions of certain elements—such as gallium, aluminum, cerium, or americium—permits the retention of the δ phase down to room temperature [1]. However, this retained δ phase is metastable with respect to eutectoid decomposition, the kinetics of which are exceedingly long [3–5,10]. Upon cooling a Pu-1.9 at.% Ga alloy below room temperature, another instability is revealed in which the metastable δ phase partially transforms to the metastable α' phase by means of a martensitic transformation. This α' phase exhibits the monoclinic α -Pu structure, but the $\delta \rightarrow \alpha'$ transformation proceeds rapidly enough to trap Ga in the lattice, expanding the lattice parameters over those of unalloyed α -Pu [5,11,12]. Between the parent δ matrix and the α' product phase, there is an approximately 20% volume difference that causes significant

elastic and plastic strains associated with the transformation. These strains likely arrest the $\delta \rightarrow \alpha'$ transformation before completion, resulting in a yield of only about 25% volume fraction of the α' product phase embedded within a δ -phase Pu-Ga matrix. Electrical resistivity, dilatometry, and differential scanning calorimetry measurements suggest that the $\alpha' \rightarrow \delta$ reversion occurs via an isothermal burst martensite mode [13–15].

Whereas the amount of transformation product of an athermal martensitic transformation is dependent only on temperature [16], the martensitic $\delta \rightarrow \alpha'$ transformation in Pu-Ga alloys proceeds isothermally, wherein both temperature and time determine the amount of transformation. A typical isothermal transformation takes on a characteristic “C” shape when the amount of transformation is plotted in a time-temperature-transformation (TTT) diagram. This “C” shape, where the “nose” temperature is the minimum in the time for the initiation of transformation, results from the competition between two mechanisms characterized by opposite temperature dependences. In the case of a diffusional, isothermal transformation, the high-temperature portion of the “C” is dominated by diffusion, the magnitude of which decreases with decreasing temperature, and the low-temperature portion of the “C” is dictated by the free energy difference (driving force) between the initial and final phases, which increases with decreasing temperature.

Somewhat atypically, the isothermal $\delta \rightarrow \alpha'$ transformation in Pu-1.9 at.% Ga exhibits two “C’s” (double-C behavior) when plotted on a TTT diagram (see Figure 1); that is, there exist two nose temperatures anchoring an upper- and lower-C at which the transformation can proceed maximally [17,18]. The energetic mechanisms responsible for the appearance of this double-C behavior are not fully known, although the free energy difference is undoubtedly involved. Double-C curves have been observed previously in U-Cr alloys [19,20], where the double-C is associated with different transformation products reminiscent of pearlite and bainite in steels. However, the curious results first reported for Pu-1.4 at.% Ga and Pu-1.9 at.% Ga alloys indicate that transformation in either portion of the double-C yields the same α' product phase. It was originally proposed by Orme *et al.* that the α' product phase formed in the upper- and lower-C through different transformation mechanisms [17]. However, from optical microscopy, Deloffre found that the α' morphologies in the upper- and lower-C of a Pu-1.9 at.% Ga alloy were nearly identical, but proposed that the α' phase in the upper-C preferentially nucleated on grain boundaries [21]. Subsequent dilatometry and calorimetry experiments suggested that the reversion of the α' phase in a Pu-1.9 at.% Ga alloy, unlike the Pu-1.2 at.% Ga alloy, occurs directly with no evidence for intermediary phases during the $\alpha' \rightarrow \delta$ transformation [22]. Recent symmetry considerations propose that the $\delta \rightarrow \alpha'$ transformation should occur with intermediary phases, although the lifetimes and dependences upon Ga concentration of these proposed intermediary phases is unclear [23].

More recently, the role that a “conditioning” treatment—an isothermal hold on the timescale of hours at temperatures below the annealing temperature but above the transformation temperature—plays in the transformation has been examined by Blobaum *et al* [24]. Differential scanning calorimetry experiments revealed that thermal cycles immediately following a high-temperature anneal resulted in only a small amount of heat released at low temperature. However, if a conditioning treatment was employed subsequent to a high-temperature anneal, but before cooling to sub-ambient temperatures, the measured heat was increased over that of the unconditioned specimen. This increase in the measured heat with conditioning was interpreted as an increase in the amount of transformation over that obtained with an unconditioned specimen. Furthermore, the results from Blobaum *et al.* show that conditioning at a temperature where the δ phase of Pu-1.9 at.% Ga is metastable is effective at promoting the $\delta \rightarrow \alpha'$ transformation. It was posited that conditioning engenders the formation of embryos of the energetically favorable α , β , or γ equilibrium phases [24]. These embryos could then serve as additional potent nucleation sites for the $\delta \rightarrow \alpha'$ transformation, although it was suggested that the proposed β and γ embryos were less effective at promoting the martensitic transformation.

The exact nature of this conditioning treatment is unconfirmed, but its effects and importance with respect to the morphology and transformation mechanisms are largely unknown. We therefore report the microstructural characterization of a Pu-1.9 at.% Ga alloy as a function of temperature, time, and conditioning. From these experiments, we illuminate the role of conditioning in the $\delta \rightarrow \alpha'$ transformation and the resulting morphologies in the upper- and lower-C. We propose that conditioning strongly influences nucleation of the $\delta \rightarrow \alpha'$ transformation, but is much less consequential to either particle growth or overall morphology.

2 Methods and Techniques

2.1 Experimental Details

A single, 3-mm-diameter specimen of a Pu-1.9 at.% Ga alloy with an initial mass of approximately 200 mg ($\approx 450 \mu\text{m}$ thick) was used for all experiments [25]. A small portion of the sample was thinned through electropolishing after each experimental condition. The thinnest section of the disc, at the end of all experiments, was approximately $200 \mu\text{m}$. The sample was originally cast in 2000, and its original composition, reported in Table 1, was analyzed with Inductively Coupled Plasma Mass Spectrometry (ICP MassSpec). The Pu-239 isotope comprises the bulk of the specimen, with ^{240}Pu as the most prevalent of

the minor isotopes. The presence of delta-stabilizing elements other than Ga was not detected, although the ICP MassSpec could not chemically resolve individual concentrations of ^{241}Pu and ^{241}Am . After 8 years of aging, the sample should have an americium content between 0.006 at.% (assuming no ^{241}Am when cast) and 0.171 at.% (assuming no ^{241}Pu when cast). While Fe is the most prevalent impurity in our sample, these impurities are expected to aggregate into Pu_6Fe impurity phases, which migrate to the grain boundaries and do not affect the Pu-Ga phase diagram [26]. Due to the radioactive decay of Pu and time since casting, slight compositional changes, particularly from in-growth of daughter products, are expected. This sample was previously used for differential scanning calorimetry experiments, where it was cycled 35 times through the $\delta \rightarrow \alpha'$ transformation and reversion as well as up to 375 °C, where it was held for 8 or more hours per cycle.

The sample was prepared for optical metallography experiments by mechanically polishing the surface with successively finer alumina lapping films as small as 3 μm . The sample was then annealed at 375 °C for 16 hours in a vacuum furnace to remove any deformation-induced phases and defects resulting from the polishing procedure [13]. The grain size of the sample was well in excess of 100 μm , of sufficient size such that M_S should be weakly dependent on grain size [27]. While no electron microprobe was performed, the micrographs revealed no Ga coring to the degree seen by Mitchell *et al.* [14], suggesting a reasonably homogeneous Ga distribution for this particular sample.

The specimen was subjected to several thermal cycles designed to probe various coordinates within the TTT diagram. A set of experiments was performed to examine the microstructures in the upper-C (-120 °C), in the lower-C (-155 °C), and below the lower-C (-196 °C). The general procedure was as follows: (1) anneal at 375 °C for 8 or more hours to remove any previously formed α' phase as well as dislocation damage from preparation or previous $\delta \rightarrow \alpha'$ transformation; (2) condition by isothermally holding the specimen at 25 °C for 8 or more hours; (3) quench to the desired temperature; (4) hold at the desired temperature for a specified time; (5) upquench to room temperature; and, finally, (6) perform optical microscopy. Step two was omitted for experiments for which no conditioning treatment was desired. For the -120 °C and -155 °C experiments, the sample was quenched from room temperature or 375 °C by rapidly placing it in bath of ethanol within a copper heat sink that was thermally sunk to a bath of liquid nitrogen contained in a dewar flask. Experiments at -196 °C were achieved by submerging the sample directly in a bath of liquid nitrogen. Upquenches were achieved by moving the sample into a beaker filled with room temperature ethanol. Cooling rates during the quenching process were estimated from the start of the quench to the time of temperature equilibration to be in excess of ≈ 500 °C/min. The temperature of the heat sink was monitored with a thermocouple or a resistive thermometer and controlled by a Lakeshore 340 temperature controller. Uncertainties

in hold times were approximately 10 seconds, and the temperature was held within 5 °C of the desired temperature.

Following each thermal cycle, the sample was electropolished at 135 V for 2 minutes in a -15 °C solution of nitric acid:ethanol:butoxyethanol (2:9:9). To enable optical contrast between the δ matrix and the α' product phase, the sample was anodized at 7 V for 30 seconds directly after the electropolishing procedure. Using a Nikon metallographic microscope, the microstructures were imaged through polarized light at different areas upon the surface with several magnifications and digitally captured. The thermal cycles, electropolishing, anodizing, and optical metallography were performed in a glovebox with a controlled atmosphere of dry nitrogen.

2.2 Image Analysis of the Micrographs

The resulting microstructures were analyzed with ImageJ software to determine the median length of the α' particles, l_m ; the areal number density of α' particles, n_a ; and the fractional amount of transformation, f . The results for l_m and n_a are tabulated in Table 2. While f is defined as an area fraction, the high-aspect ratio of the particles combined with statistical sampling make f a reasonable approximation to the volumetric amount of transformation [28]. The analysis was performed on images acquired at various locations on the sample (including multiple grains) after each thermal cycle. The aforementioned quantities are reported as averages plus or minus standard deviations. It should be noted that the standard deviation does not solely correspond to experimental uncertainty, but instead reflects both the natural distribution of particles and measurement errors.

The images were processed by bandpass filtering the image to smooth the contrast in background variance, which occurred on a length scale of approximately 1 μm ($\sim 3 \mu\text{m}^2$). After the filtering process, the image was subjected to a threshold process to distinguish the α' particles from the filtered background. A native, particle-detection routine was then applied to the adjusted images; the particles were defined as areas of constant contrast subtended by a closed contour. In order to neglect impurity phases—present even in untransformed microstructures and typically rounder than the α' particles—and particles not wholly contained within the image borders, the routine was set to ignore particles that were nearly circular or particles that extended to the boundaries of the image. The length, l_i , and area, A_i , of each detected particle was returned by the routine.

The least accurate quantity determined through the above analysis was the value of n_a , whose accuracy suffered from several problems. The detection limit

of the routine was approximately equal to the background contrast variance ($3 \mu\text{m}^2$), thus particles smaller than this limit were not counted. In addition, on the scale of the acquired micrographs, particles often appeared to intersect, meaning particles in close proximity could have been misidentified as a single particle and undercounted. The values of n_a have been nonetheless reported in units of thousands of particles/ mm^2 for comparison, but they should be regarded as estimates. While the analysis of each image resulted in many values of l_i and A_i , the number of particles returned from any image was a single quantity. As such, the statistics behind n_a were based on the number of images analyzed as opposed to the number of particles detected; this fact manifested the large standard deviations of n_a .

Inaccuracies in l_i derived from the same shortcomings that limited the accuracy of n_a , specifically the problem associated with intersecting or proximal particles. In the case of l_m , however, there were many particles detected for each experimental condition. Thus the accuracy of l_m was improved over n_a by means of better statistics. Particle lengths have been reported in μm .

Finally, the fractional transformation $f = \frac{\sum_{i=1}^n A_i}{A_{img}}$ was the most robust of the three quantities obtained from the ImageJ analysis because it was determined as the proportion of the number of pixels within a range of contrast defining the α' particles to the total number of pixels in a given image (A_{img}). This proportion has been given in percent. Like l_m , f also benefited from the improved statistics associated with a large statistical sample size.

3 Results

Example micrographs corresponding to hold temperatures of -120, -155, and -196 °C are shown respectively in Figures 2–4. In these micrographs, the α' phase can be seen clearly as high aspect ratio, black or white particles embedded within the δ matrix. The contrast (*i.e.*, the brightness/darkness on a grayscale) of the α' particles with respect to the δ matrix is a result of the polarization of the light and the anodizing process, the results of which are a function of particle size, crystallographic orientation, and inclination with the surface. In addition to the α' particles evident in the microstructure, impurity phases are seen as either dark or bright elliptical objects and grain boundaries are discerned by dark, irregular lines often associated with changes in large-scale contrast. The α' particles remain highly acicular for all experimental conditions and they grow within a single grain with only a few variants, as discussed in previous studies [29,30].

3.1 *Conditioning-enhanced Transformation in the Upper-C at -120 °C*

The results of our microstructural characterization of the $\delta \rightarrow \alpha'$ transformation in the upper-C are displayed in Figure 2. Figures 2a and 2b reveal little quantitative or qualitative discrepancy between the experiments with and without prior ambient-temperature conditioning when held at -120 °C for 30 seconds: $f=4.3\pm1.4$ and $3.3\pm1.5\%$, respectively, while $n_a=8.4\pm4.5 \times 10^3$ and $7.1\pm2.9 \times 10^3$ particles/mm², respectively. On the contrary, as seen in Figures 2c and 2d, a 4-hour isothermal hold at -120 °C is sufficient to reveal significant conditioning-induced differences in the microstructure resulting from the $\delta \rightarrow \alpha'$ transformation (with and without conditioning, respectively, $f=8.8\pm3.0$ and $2.1\pm2.2\%$ with $n_a=26.3\pm7.0 \times 10^3$ and $4.4\pm1.3 \times 10^3$ particles/mm²). Without conditioning, there appears to be no increase in the amount of transformation between a 30-second and 4-hour isothermal hold (Figures 2a and 2c); however, with conditioning, a 4-hour isothermal hold produces a significant increase in the amount of transformation and the areal number density of particles (Figures 2b and 2d). For an intermediate hold time of one hour following conditioning (not shown), $f=7.9\pm2.5\%$ and $n_a=16.9\pm10.1 \times 10^3$ particles/mm², values between those of the 30-second and 4-hour hold times.

Without conditioning, the formation of α' in the upper-C appears time independent on the time scale investigated. However, provided the sample undergoes a conditioning treatment prior to cooling, these micrographs imply time-dependent formation of the α' martensite, as would be expected from the isothermal TTT diagram for Pu-1.9 at.% Ga. These differences between the microstructures with and without conditioning suggest that conditioning *enhances* the nucleation or growth of the α' product phase in the upper-C.

3.2 *Conditioning-enabled Transformation in the Lower-C at -155 °C*

Figure 3 shows characteristic microstructures resulting when the $\delta \rightarrow \alpha'$ transformation proceeds at -155 °C (in the lower-C) with and without prior conditioning treatments. Of immediate note is the fact that, without conditioning, no transformation products are resolved with optical microscopy for either the 30-second or the 4-hour hold times (Figures 3a and 3c). With conditioning, the result is quite different (Figures 3b and 3d), where it appears that conditioning *enables* transformation in the lower-C. The previously conditioned 30-second and 4-hour hold times produce similar amounts of transformation in excess of that seen in the upper-C, with $f=12.4\pm2.0$ and $12.7\pm3.7\%$, respectively. The lack of an obvious increase in the amount of transformation as a function of hold time does not in itself confirm or contradict the isothermal nature of the

transformation in the lower-C; however, the nearly time-independent value of f at -155 °C does not quantitatively agree with the kinetics proposed by Orme, Faiers, and Ward [17]. In fact, such a nearly time-independent amount of transformation intimates that, with prior conditioning, the transformation may proceed athermally at -155 °C.

For the 30-second hold time at -155 °C, $n_a=12.9\pm0.5 \times 10^3$ particles/mm², while $n_a=7.8\pm3.9 \times 10^3$ particles/mm² for the 4-hour hold time. While it appears that the value of n_a decreases significantly with increased hold time, the small statistical sample size for the 30-second isothermal hold images likely results in incomplete statistics. These incomplete statistics combined with the inherent inaccuracy in n_a prohibit conclusively ascribing a trend with increasing hold time to the changes in n_a at -155 °C.

4 Discussion

4.1 Character of the Transformation at -155 °C

Mindful of the results detailed in Section 3.2, a set of experiments was performed at -196 °C to clarify whether the transformation at -155 °C proceeds with an athermal component. Example microstructures are presented in Figure 4. Without conditioning, a 30-second hold following a quench to -196 °C yields no transformation (Figure 4a). A subsequent measurement was performed in which the specimen was conditioned, quenched to -196 °C, and held for 4 hours (Figure 4b). No particles were detected with this treatment. If the transformation at -155 °C were athermal, then α' particles would be present in the resultant microstructures of Figure 4. As no particles were detected, it is unlikely that there is an athermal component to the transformation at -155 °C. Furthermore, the lack of particles in Figure 4b implies that there is no isothermal transformation occurring at these low temperatures, since one would expect an increase in transformation with increasing hold time. It is speculated that the transformation at -155 °C is isothermal in character with strong time-dependent nucleation or growth at short time scales.

4.2 Particle Statistics and Distributions of the α' Phase

The particle statistics presented in this section have been extracted from multiple images (varying from 4 to 15) for each experimental condition. The collection of images for each time/temperature/conditioning combination encompasses multiple grains. Because the α' particles were not observed to cross

grain boundaries in this study, each individual grain represents an independent sampling of the particle distributions. These independent grains, however, were all subjected to the same thermal treatment and should be compositionally similar. The images acquired from each experimental condition have been quantitatively analyzed, the results of which are displayed in Figures 5 and 6, where the data are represented as histograms displaying the probability of a particle growing to a given area and length, respectively. The median particle length l_m is given in each pane of Figure 6. These distributions provide a quantitative comparison between the differences and similarities of the development of the α' phase in the upper- and lower-C. While the morphologies appear similar, subtle details regarding the formation of the α' product can be extracted from the probability distributions. Previously unpublished optical micrographs from a different sample (but the same compositional alloy) held at -120 °C for 11 hours yield distributions, areal number densities, and fractional transformations consistent with those reported here.

The growth of an individual α' particle is expected to proceed stochastically from a viable nucleation site, where an individual particle is expected to grow to a size ultimately governed by properties of its local environment including strain fields, defects, and grain boundaries. The probability distribution of such a random growth process is expected to be described by a distribution within the exponential class. Such a distribution should be bounded so that there is zero probability of discovering a particle with zero area, a concept lacking physical significance. Commonly used distributions satisfying these conditions are the log-normal and gamma distributions, both of which have been used to describe grain size [31]. When displayed as a semi-log plot, the distributions obtained from the image analysis do not evince any tendency for gaussian behavior, as would be expected for a log-normal distribution. As such, the more general of the aforementioned distributions, the gamma distribution, is used to describe the histograms of Figures 5 and 6.

Using the gamma distribution, the probability $\mathcal{P}(A)$ of a particle growing to an area A can be described by:

$$\mathcal{P}(A) = A^{b-1} \frac{e^{-A/c}}{c^b}, \quad (1)$$

where b and c are fitting parameters related to the shape and size factor of the distribution, respectively. When $b = 1$, the gamma distribution collapses to the exponential distribution. The data have been normalized and fit with equation 1 such that the area under the probability distribution function is equal to one. The results of these fits are delineated in Figure 5 and in Table 2.

Similarly, the probability $\mathcal{P}(l)$ of a particle growing to length l can be described

by a gamma distribution; however, the data for l display clear maxima in all of the distributions. Using the boundary condition that the distribution be maximal at the mode length l_0 , the gamma distribution can be reduced to a function of a single free parameter, arbitrarily chosen as l^* :

$$\mathcal{P}(l) = l^\delta \frac{e^{-l/l^*}}{l^{*(\delta+1)}}, \quad (2)$$

where $\delta \equiv l_0/l^*$. The values of l^* are displayed in the figure panes and in Table 2. The utility of using equation 2 to describe the length distribution lies in the ability to extract a characteristic length scale, l^* , for each thermal treatment.

Equation 1 provides a good fit for all of the histograms of Figure 5 except for Figure 5g, where deviations are likely a product of a small statistical sample size (fewer images for this treatment). For the cases of Figures 5d and 5e, the lack of detectable small particles combined with the values of c prohibit the determination of b . As such, the results obtained from the distributions in Figures 5d and 5e are presented as upper limits. In general, increasing hold times in the upper-C yields a distribution that becomes significantly weighted toward small particles, as indicated by the reduction in c . The lower-C shows a somewhat opposite trend, with increasing hold times having little effect on the low-area portion of the distribution. The value of c appears to increase with increasing hold times in the lower-C, but higher magnifications from SEM or TEM are necessary to quantify the low-area portion of the distributions.

By analyzing the probability distributions and extrapolating toward low particle areas, the expected area occupied by particles below the detection limit can be estimated. The areas corresponding to particles expected to exist below this limit are represented by the shaded regions in each pane of Figure 5. Depending on the specifics of the distribution function and assuming the validity of such a distribution, the inaccuracy of the measured fractional transformation f (displayed in Figures 2–4) can be extreme. For the limiting case of Figure 5e (associated with the micrograph in Figure 2d), the measured area could account for as little as 51.1% of the transformation product, while the optically undetectable portion of the distribution A_m would then correspond to 48.9% of the total amount of $\delta \rightarrow \alpha'$ transformation. The values of A_m , given in percent as a proportion to the total distribution, can be used to revise our estimate for the fraction of transformation, defined as f_r and given in Figure 5 and Table 2.

Transformations in the upper-C (Figures 6a–6e) tend to have very similar length distributions, with the caveat that the median length is reduced for the conditioning-*enhanced* transformation products with 1-hour and 4-hour holds following conditioning. The decrease in the median length of the particle with increased holding time is likely a consequence of the burst nature of

the transformation: as α' particles continually form within the δ matrix, they occupy more space and produce plastic deformation in their immediate vicinity, preventing future particles from growing to large dimensions. The length distributions echo the results of the area distributions and the dissimilarities between the upper- and lower-C. Increasing hold times in the upper-C fills in the low-particle-length region of the distribution. In the lower-C more long particles form with increasing hold time, while the low-particle-length region of the distribution remains substantially equivalent. Instead of decreasing as in the upper-C, the median particle length in the lower-C increases slightly with increasing hold times. The values of l^* extracted from the fits are similar in the upper-C regardless of conditioning, with an average value of approximately $2.33 \mu\text{m}$. This relative insensitivity to the presence of conditioning may indicate that growth of the α' phase is not affected by conditioning, which may further suggest that conditioning alters the nucleation processes of the $\delta \rightarrow \alpha'$ transformation.

4.3 Relationship with Previous Work

Previous work by Orme, Faiers, and Ward used dilatometry to determine the TTT diagram for Pu-1.9 at.% Ga, where the nose of the upper-C is near -130°C and the nose of the lower-C is closer to -155°C [17]. Since the effects of conditioning have been shown to saturate in only 8 hours [24], it is likely that the specimen measured by Orme *et al.* was unintentionally conditioned. As such, their TTT diagram is probably representative of a conditioned sample and any comparisons to the data herein should account for this fact. Indeed, the revised fractional transformation f_r of isothermal holds at -120°C following a conditioning treatment are in reasonable agreement with this previous work: a 30-second hold produces about 5% transformation, a 1-hour hold produces about 11% transformation, and a 4-hour hold produces about 13% transformation. About 5°C above the nose of the upper-C determined by Orme *et al.*, the $\delta \rightarrow \alpha'$ transformation appears to proceed as follows: a 30-second hold yields less than 5% transformation, a 1-hour hold yields slightly in excess of 10% transformation, and a 4-hour hold could be expected to yield between 10% and 15% transformation. The evolution of f_r may suggest that the nose of the TTT diagram, at least for our particular sample, is at a slightly elevated temperature with respect to that of Orme *et al.*

When f_r for the lower-C is examined, the case for compatibility with previous work is not so clear. Qualitatively, the transformation appears to be isothermal, as previously mentioned (Section 4.1); however, the quantitative evolution of f_r is inconsistent with the TTT diagram of Orme *et al.*, where the fractional transformation was found to evolve comparably to that of the upper-C. Our data suggest that the isothermal transformation proceeds in

the lower-C at a much greater initial rate, which is reflected by the large value of $f_r \approx 14\%$ after a 30-second hold at -155°C . Deloffre used density as a measure of the amount of α' formed, but his values of 5% transformation after 30 minutes at -110 and -180°C are outside the temperature range of this study and the study of Orme *et al* [17,21]. These differences could be due to discrepancies in the definition of $t = 0$, quench rate, thermal equilibration, or sample-dependent impurities such as defects, helium bubbles, or decay products from the nuclear decay of Pu. A more thorough mapping of the TTT diagram with and without conditioning will be necessary to address these considerations.

Accompanying the original discovery of the double-C was the proposal that the upper- and lower-C yield the α' phase via different isothermal transformation mechanisms: a massive transformation for the upper-C and a martensitic transformation for the lower-C [17]. The morphologies of the α' product phase in the upper- and lower-C appear identical within the limits of optical microscopy (as seen by Deloffre [21]); the α' phase remains highly acicular in both regions of the TTT diagram. As such, there is no clear distinction from the microstructure that would suggest that the transformation proceeds via different mechanisms in the upper- and lower-C. Furthermore, the α' particles are not seen to grow through grain boundaries, a ubiquitous phenomenon associated with massive transformations [32,33]. Therefore, a massive transformation is an unlikely mechanism for the $\delta \rightarrow \alpha'$ transformation in either the upper- or lower-C.

Previous work by Deloffre indicated that a Pu-1.2 at.% Ga alloy exhibited two different morphologies in the upper- and lower-C: plate-shaped and lenticular, respectively [21,22]. From x-ray diffraction, the presence of a short-lived γ' phase was seen in the upper-C of a Pu-1.2 at.% Ga alloy, and this phase appeared in the same plate-shaped morphology of the α' phase [21]. Furthermore, he suggested that the upper-C transformation in a Pu-1.2 at.% Ga alloy was partly indirect, with a portion of the $\alpha' \rightarrow \delta$ reversion proceeding consecutively through the β and γ phases before ultimately returning to the δ phase above 350°C . However, no intermediate phases were reported in the $\alpha' \rightarrow \delta$ reversion, the upper-C, or the lower-C of a Pu-1.9 at.% Ga alloy. While the optical microscopy presented herein cannot address the reversion of the α' phase, no evidence for a plate-shaped γ' phase is seen, consistent with the results of Deloffre. Similar to Deloffre's previously published work, the micrographs of Figures 2 and 3 reveal the same morphology for transformations occurring in the upper- and lower-C. It was noted by Deloffre that, in a Pu-1.9 at.% Ga alloy, α' particles preferentially nucleate at grain boundaries in the upper-C, while showing no propensity for any particular nucleation site in the lower-C. Although α' particles intersect grain boundaries in the upper- and lower-C, this study lacks the time resolution to conclusively confirm or deny Deloffre's supposition of preferred nucleation in the upper-C.

4.4 Implications for the Nature of Conditioning

The microstructures presented in Figures 2 and 3 show that conditioning has profound effects on the evolution of the $\delta \rightarrow \alpha'$ phase transformation. While previous differential scanning calorimetry measurements indicated an increase in the amount of transformation product with conditioning, those measurements were performed with a cooling rate too slow to separate the effects of conditioning in the upper- and lower-C of the TTT diagram [24]. That the lower-C appears to be enabled by a conditioning treatment may be a key piece of evidence toward identifying the nature of conditioning. If conditioning were simply an annealing process, it is difficult to surmise how it is capable of enabling transformation in the lower-C. Furthermore, while the upper- and lower-C do display slight disparities in their size distributions, the time-dependent evolution of the distributions, as seen in the upper-C, does not appear to be greatly affected by conditioning. This would suggest that conditioning does not affect dramatically the growth of the α' phase, but rather it facilitates the development of additional nucleation sites.

One avenue for increasing the number of nucleation sites could be the accumulation of radiation-induced damage in the lattice during conditioning. Perhaps, through Pu self-irradiation, dislocations form, persist, and serve as nucleation centers at low temperatures, thus increasing the number of observed α' particles and the volumetric amount of transformation. However, it was shown by Fluss and co-workers that most radiation damage is annealed out near room temperature [8]. Blobaum *et al.* found that conditioning exhibits a maximal efficacy at promoting the $\delta \rightarrow \alpha'$ transformation at room temperature, with low-temperature conditioning treatments resulting in smaller amounts of transformation than those at room temperature [24]. If damage through self-irradiation were the underlying principle responsible for conditioning, then one would expect a temperature-dependent conditioning effect that increases with decreasing temperature, a dependence not observed experimentally. The mass transport phenomena, including radiation-enhanced diffusion, of self-irradiation and how they might affect the $\delta \rightarrow \alpha'$ transformation in Pu-Ga alloys are certainly not fully understood, and, in order to fully explore the potential for radiation damage as a description of conditioning, measurements using different Pu isotopes with more or less specific activity than ^{239}Pu would be desirable.

Another method for increasing nucleation sites could be the formation of second-phase embryos or nuclei during the conditioning treatment [24]. At room temperature, a Pu-1.9 at.% Ga alloy should be in a phase-separated equilibrium structure of $\alpha + \text{Pu}_3\text{Ga}$, but the δ -Pu phase is retained due to very slow kinetics (of order 10,000 years [3–5,10]) for this eutectoid decomposition. Nevertheless, there exists a driving force for the δ phase to decompose,

and stable α or Pu_3Ga nuclei could form. The short time scales of conditioning, near 8 hours, would tend to prohibit the formation of Pu_3Ga nuclei in a homogenized Pu-1.9 at.% Ga alloy, because significant Ga diffusion would need to occur. Therefore, it is possible that α embryos or nuclei form during the conditioning treatment. These conditioning-induced embryos or nuclei could then serve as the progenitor nuclei or heterogeneous nucleation sites for the formation α' particles at low temperature. While speculative, the presence of these progenitor nuclei could account for the rapid, conditioning-induced formation of the α' phase in the lower-C, because only growth, which has been shown to exhibit rapid burst behavior [13–15], is required in such a scenario.

If nucleation of equilibrium phases is culpable for the conditioning effect in Pu-Ga alloys, then there should be a temperature dependence to the conditioning effect that displays a maximum, which has been observed near room temperature[24]. This temperature dependence would be a function of parameters like the chemical driving force, strain energy, migration barrier, etc. Furthermore, nucleation of equilibrium phases should be insensitive to the isotope of Pu used in synthesizing the Pu-Ga alloys, provided that the activity of an isotope other than ^{239}Pu does not significantly alter the Pu-Ga phase diagram. Measurements of properties sensitive to the $\delta \rightarrow \alpha'$ transformation (differential scanning calorimetry, resistivity, dilatometry, TEM, etc.) as a function of conditioning temperature as well as Pu isotope should be capable of testing this hypothesis.

5 Conclusions

Microstructural evidence reveals that ambient-temperature conditioning has dramatic effects on the $\delta \rightarrow \alpha'$ transformation, where conditioning *enhances* the transformation at -120 °C while *enabling* the transformation at -155 °C. The isothermal nature of the transformation at -120 °C (within the upper-C of the TTT diagram) is confirmed by the time-dependent evolution of the amount of transformation. In addition, experiments involving rapid quenches to -196 °C imply that the transformation at -155 °C (within the lower-C of the TTT diagram) is also isothermal. However, the amount of transformation in the lower-C is found to be weakly time-dependent between 30 seconds and 4 hours, suggesting rapid formation of the α' phase at low times. No evidence for a massive transformation, particularly particle growth through grain boundaries, was seen in either the upper- or lower-C of the TTT diagram.

The microstructures in the upper- and lower-C appear similar, but small disparities can be identified through analysis of the size distributions of the resulting α' particles. The upper- and lower-C appear to differ in that transformation in the lower-C tends to yield larger particles. Conditioning does

not seem to affect the growth of the α' particles, intimating a change in the nucleation processes as the nature of conditioning. It is likely that conditioning promotes the formation of embryos or nuclei of equilibrium phases, which serve as nucleation sites or potent nuclei in addition to those isothermally formed at low temperature. The presence of these conditioning-induced nuclei or embryos would result in an increase in the amount of transformation when the specimen undergoes the $\delta \rightarrow \alpha'$ transformation. Further temperature- and isotope-dependent measurements should be performed to clarify the nature of conditioning in Pu-Ga alloys.

Acknowledgments

Lawrence Livermore National Laboratory is operated by Lawrence Livermore National Security, LLC, for the U.S. Department of Energy, National Nuclear Security Administration under Contract DE-AC52-07NA27344.

References

- [1] Ellinger FH, Land CC, Struebing VO. J Nucl Mater 1964;12:226.
- [2] Chebotarev NT, Smotriskaya ES, Andrianov MA, Kostyuk OE. In: Blank H, Lindner R, editors. Plutonium 1975 and other actinides. Amsterdam: North Holland; 1976. p.37.
- [3] Hecker SS, Timofeeva LF. Los Alamos Sci 2000;26:244.
- [4] Timofeeva LF. In: Mallinson LG, editor. Aging studies and lifetime extension of materials. New York (NY): Kluwer Academic/Plenum Press; 2001. p.191.
- [5] Hecker SS, Los Alamos Sci 2000;26:291.
- [6] Kubota A, Wolfer WG, Valone SM, Baskes MI, J Computer-Aided Mater Des 2004;14:367.
- [7] Wolfer WG, Los Alamos Sci 2000;26:275.
- [8] Fluss MJ, Wirth BD, Wall M, Felter TE, Caturla MJ, Kubota A, Diaz de la Rubia T, J Alloy Compd 2004; 368:62.
- [9] Hecker SS, Metall Mater Trans A 2008;39A:1585.
- [10] Turchi PEA, Kaufman L, Zhou S, Liu Z-K. J Alloy Compd 2007;444-445:28.
- [11] Olson GB, Adler PH. Scripta Metall 1984;18:401.
- [12] Heiple CR, Carpenter SH. Metall Mater Trans A 1992;23A:779.

- [13] Blobaum KJM, Krenn CR, Mitchell JN, Haslam JJ, Wall MA, Massalski TB, Schwartz AJ. Metall Mater Trans A 2006;37A:567.
- [14] Mitchell JN, Gibbs FE, Zocco TG, Pereyra RA. Metall Mater Trans A 2001;32A:649.
- [15] Schwartz DS, Mitchell JN, Pete DV, Ramos M. JOM-J Min Met Mater Soc 2003;55:28.
- [16] Delay L. In: Chan RW, Haase P, Kramer EJ, editors. Materials science and technology, a comprehensive treatment, volume 5, Phase transformations in materials. New York (NY): VCH Publishers, 1991. p.384.
- [17] Orme JT, Faiers ME, Ward BJ. In: Blank H, Lindner R, editors. Plutonium 1975 and other actinides. Amsterdam: North Holland, 1975. p.761.
- [18] Oudot B, Blobaum KJM, Wall MA, Schwartz AJ. J Alloy Compd 2007;444-445:230.
- [19] Townsend RD, Burke J. Nature 1965;205:794.
- [20] Rehtien JJ, Nelson RD. Metall Mater Trans B 1973;4B:2755.
- [21] Deloffre P, Ph.D. Thesis, University of Paris, France 1997.
- [22] Deloffre P, Truffier JL, Falanga A. J Alloy Compd 1998;271-273:370
- [23] Lookman T, Saxena A, Albers RC. Phys Rev Lett 2008;100:145504.
- [24] Blobaum KJM, Krenn CR, Wall MA, Massalski TB, Schwartz AJ. Acta Mater 2006;54:4001.
- [25] This sample is from the same batch of samples used in reference [24]. However, recent chemical analysis reveals that the chemical composition is closer to 1.9 at.% Ga than 2.0 at.% Ga.
- [26] Moore KT, Wall MA, Schwartz AJ, J Nucl Mater 2002;306:213.
- [27] Adler PH, Olson GB, Metall Trans A 1988;19A:2705.
- [28] Russ JC, Dehoff RT. Practical stereology. New York (NY): Springer, 2000.
- [29] Zocco TG, Stevens MF, Adler PH, Sheldon RI, Olson GB. Acta Mater 1990;38:2275.
- [30] Moore KT, Krenn CR, Wall MA, Schwartz AJ. Metall Mater Trans A 2007;38A:212.
- [31] Vaz MF, Fortes MA. Scripta Metall 1988;22:35.
- [32] Massalski TB. Metall Mater Trans A 1984;15:421.
- [33] Aaronson HI. Metall Mater Trans A 2002;33:2285.

Table 1

Compositional analysis of the Pu-1.9 at.% Ga specimen used. Amounts are given in atomic percent (at.%) where detected, otherwise elements not detected are indicated by a dash (“-”).

Element	Amount	Element	Amount	Element	Amount
Al	-	Ga	1.9	^{235}U	0.0081
V	0.0045	Y	-	^{237}Np	0.0011
Cr	-	Ta	-	^{238}UPu	0.013
Mn	-	W	-	^{239}Pu	93.8
Fe	0.1755	^{232}Th	-	^{240}Pu	6.00
Ni	0.0371	^{233}U	-	$^{241}\text{PuAm}$	0.174
Cu	-	^{234}U	0.0003	^{242}Pu	0.047

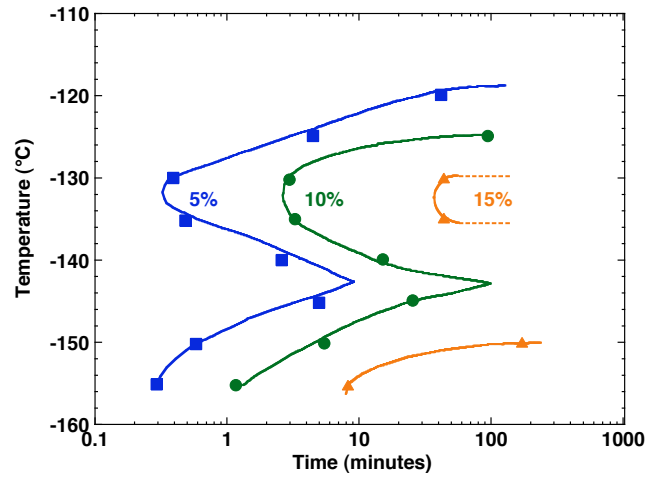


Fig. 1. The TTT diagram of the $\delta \rightarrow \alpha'$ martensitic transformation in Pu-1.9 at.% Ga (reproduced from [17]).

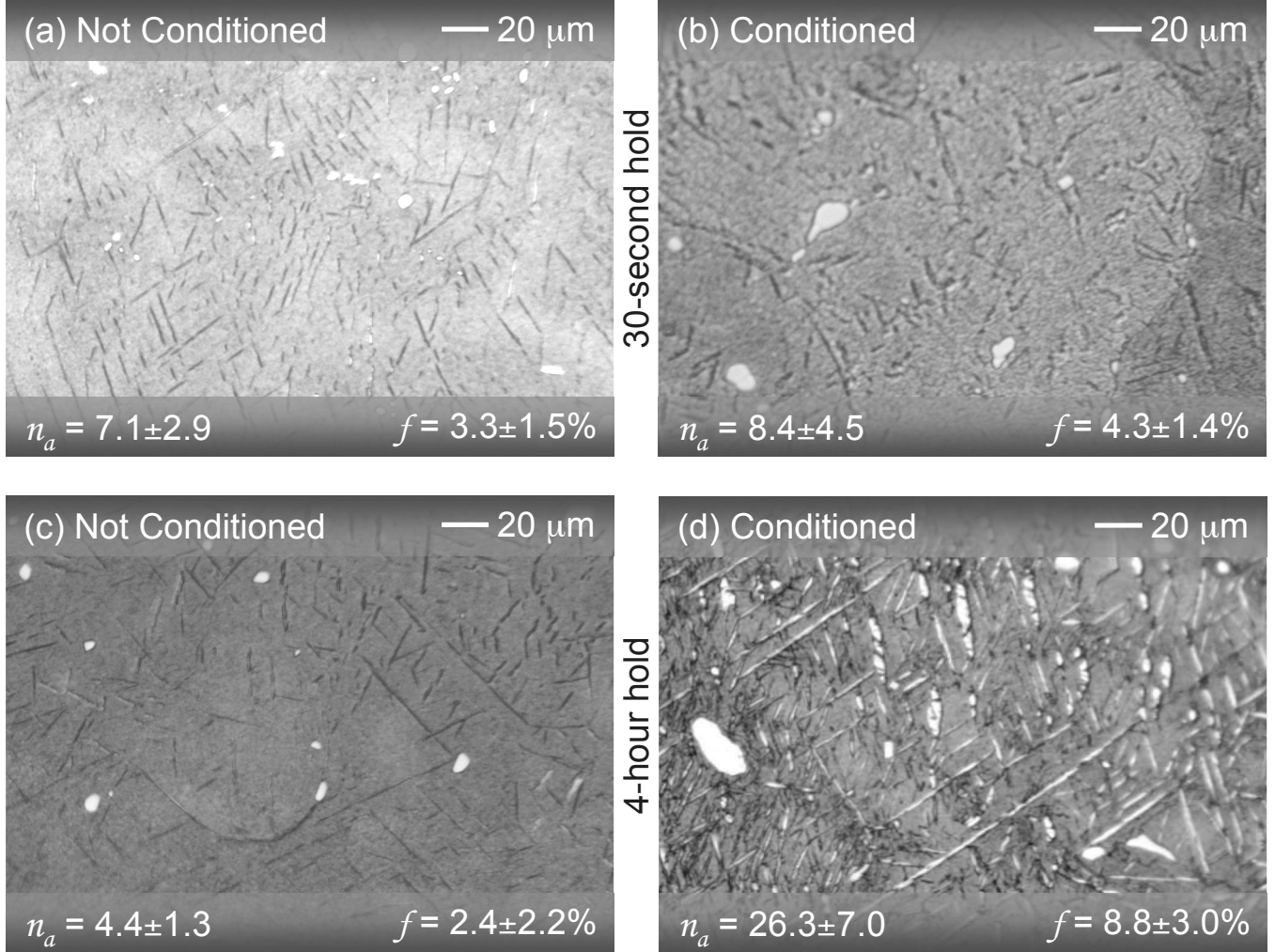


Fig. 2. The microstructure of the transformation for 30-second isothermal holds at -120 °C (a) without and (b) with conditioning and for 4-hour isothermal holds at -120 °C (c) without and (d) with conditioning. n_a is given in thousands of particles/mm².

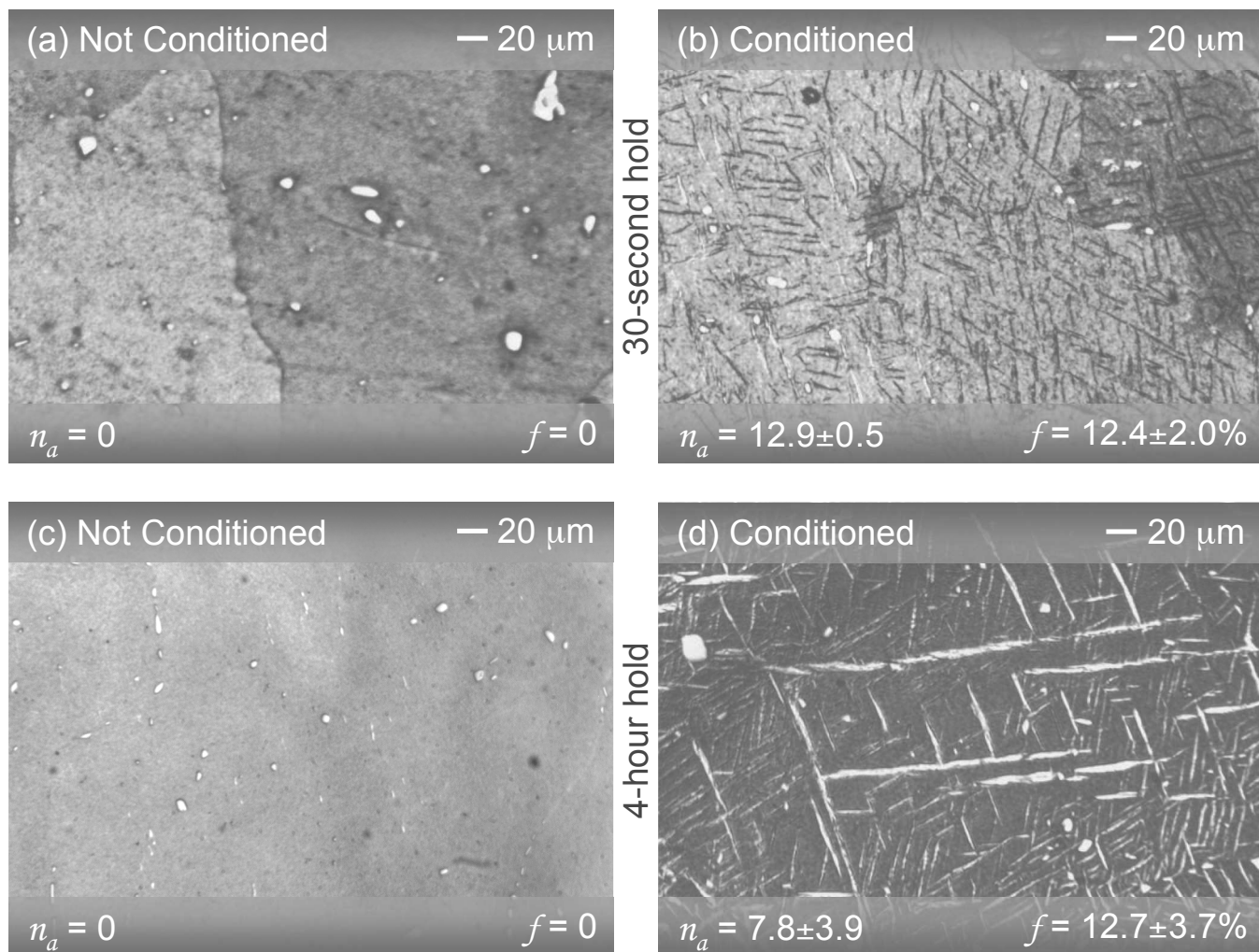


Fig. 3. The microstructure of the transformation for 30-second isothermal holds at -155 °C (a) without and (b) with conditioning and for 4-hour isothermal holds at -155 °C (c) without and (d) with conditioning. n_a is given in thousands of particles/mm².

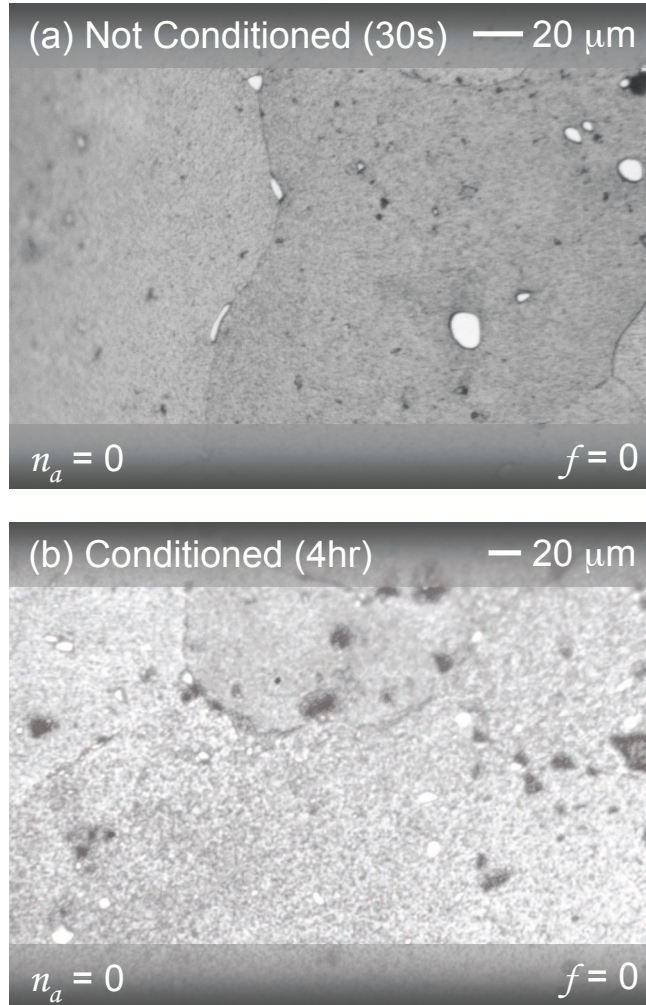


Fig. 4. The microstructure of the transformation for (a) a 30-second isothermal hold at $-196\text{ }^{\circ}\text{C}$ without conditioning and (b) a 4-hour isothermal hold at $-196\text{ }^{\circ}\text{C}$ with conditioning.

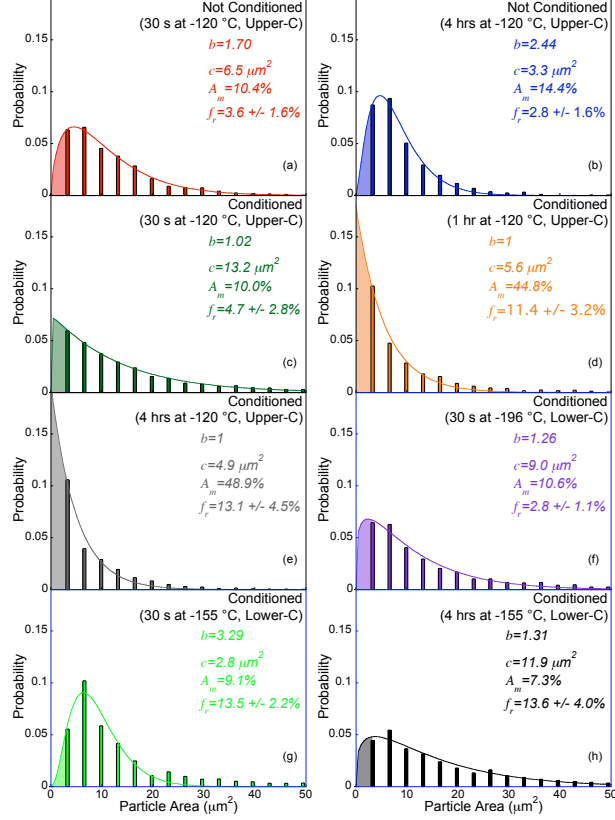


Fig. 5. (color online) Probability distributions for particles of a given area. The fraction of particle area not detected due to experimental limits (see text for details) is represented by the shaded region on the left. The solid lines are fits to equation 1 and the values of b , c , A_m , and f_r are described in the text.

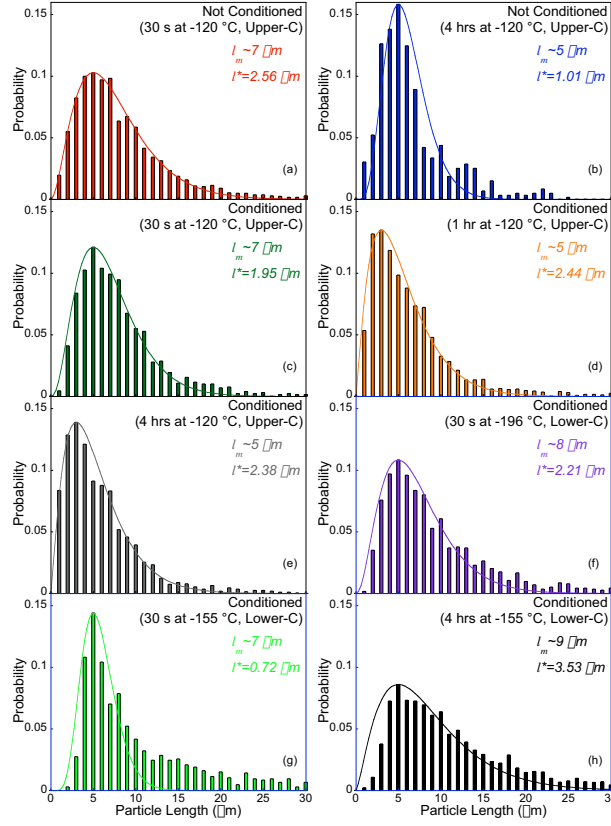


Fig. 6. (color online) Probability distributions of α' particle lengths. The solid lines are fits to equation 2 described in the text. The median length l_m and l^* are given for each distribution

Table 2

Quantities determined from the analysis of the microstructures presented in Figures 2–4: median particle length l_m in μm , areal number density n_a in 10^3 particles/ mm^2 , revised fractional transformation f_r in percent, b from equation 1, c from equation 1 in μm^2 , and l^* from equation 2 in μm . “NC” and “C” represent experiments without and with conditioning, respectively. The experimental conditions corresponding to the panes of Figures 5 and 6 are listed in the second column.

		l_m	n_a	f_r	b	c	l^*
NC, 30 s, -120 °C	(a)	7	7.1 ± 2.9	$3.6\pm 1.6\%$	1.70	6.5	2.56
NC, 4 hr, -120 °C	(b)	5	4.4 ± 1.3	$2.8\pm 1.6\%$	2.44	3.3	1.01
C, 30 s, -120 °C	(c)	7	8.4 ± 4.5	$4.7\pm 2.8\%$	1.02	13.2	1.95
C, 1 hr, -120 °C	(d)	5	16.9 ± 10.1	$11.4\pm 3.2\%$	1	5.6	2.44
C, 4 hr, -120 °C	(e)	5	26.3 ± 7.0	$13.1\pm 4.5\%$	1	4.9	2.38
C, 30 s, -196 °C	(f)	8	1.4 ± 0.7	$2.8\pm 1.1\%$	1.26	9.0	2.21
C, 30 s, -155 °C	(g)	7	12.9 ± 0.5	$13.5\pm 2.2\%$	3.29	2.8	0.72
C, 4 hr, -155 °C	(h)	9	7.8 ± 3.9	$13.6\pm 4.0\%$	1.31	11.9	3.53
NC, 30 s, -155 °C	-	-	0	0	-	-	-
NC, 4 hr, -155 °C	-	-	0	0	-	-	-